Jürgen Ackermann; Tilman Bünte

Robust prevention of limit cycles for robustly decoupled car steering dynamics

Kybernetika, Vol. 35 (1999), No. 1, [105]--116

Persistent URL: http://dml.cz/dmlcz/135271

KYBERNETIKA — VOLUME 35 (1999), NUMBER 1, PAGES 105 - 116

ROBUST PREVENTION OF LIMIT CYCLES FOR ROBUSTLY DECOUPLED CAR STEERING DYNAMICS

JÜRGEN ACKERMANN AND TILMAN BÜNTE

Considerable safety benefits are achieved by robustly decoupling the lateral and yaw motions of a car with active steering. Robust unilateral decoupling requires an actuator to generate an additional front wheel steering angle. However, introducing actuators to closed loop systems may cause limit cycles due to actuator saturation and rate limits. Such limit cycles are intolerable w.r.t. safety and comfort. By introducing a simple nonlinear modification of the control law, this paper proposes a remedy to significantly reduce the susceptibility to limit cycles for robustly decoupled car steering dynamics. The robustness of the resulting system w.r.t. the avoidance of limit cycles is investigated for varying operating conditions by combining the parameter space approach and the theory of describing functions.

1. INTRODUCTION

Practical driving tests have shown essential safety advantages for a robust steering control law which is based on feedback of the yaw rate into active front wheel steering [3]. By the control law, robust unilateral decoupling of the lateral and yaw motions of the car is achieved. The task of driving a car then simplifies to keeping a point mass on the track by commanding its lateral acceleration. Yaw disturbances e. g. from crosswind, flat tire, or asymmetric braking forces are attenuated by the robust decoupling control law for low frequencies. It requires an actuator to generate an additional front wheel steering angle. The actuator needs to be equipped with a rate limiter for overload protection. However, the introduction of nonlinear elements makes the closed loop susceptible to limit cycles. One means to investigate limit cycles is the approximation of the nonlinear part by a sinusoidal-input describing function (DF) [5]. On the other hand, for linear robust controller design and robust stability analysis of controlled plants, the parameter space approach [1] is a suitable method. This paper is concerned with proving the robust prevention of limit cycles for robustly decoupled steering dynamics by combining the DF theory with the parameter space approach. Particularly, the benefit from introducing a saturation into the controller is studied.

Section 2 and Appendix A introduce a simple linear car model which is sufficient for the subsequent analysis. Various aspects of the robustly decoupling control law

and of one of its modifications [2] are recapitulated in Section 3. A generic feedback system is defined to allow an investigation of different controller versions by simply setting respective parameters. Section 4 offers a brief summary of the DF theory, because it will be used in the sequel. The insertion of a saturation into the controller is proposed in Section 5 and it is illustrated how thereby the susceptibility to limit cycles can be reduced. Section 6 is dedicated to the robustness analysis w.r.t. the prevention of limit cycles. For various controller versions, an actuator bandwidth is specified. The application of the parameter space method then allows to verify the robust prevention of limit cycles for an entire operating domain.

2. CAR MODEL

The employed linear second order car model is described in Appendix A. Input to the model is the front wheel steering angle δ_f and the outputs are yaw rate r and lateral acceleration at the front axle a_f. Introducing a gain parameter K and a gain scheduling by the car velocity v, let h be an auxiliary output variable defined by

$$h = r + \frac{K}{v} a_f. \tag{1}$$

Equations (11) - (14) and (1) yield the vehicle transfer function from δ_f to h:

$$G_v(s) = \frac{h(s)}{\delta_f(s)} = \mu c_{f0} \frac{e_0 + e_1 s + e_2 s^2}{f_0 + f_1 s + f_2 s^2} \tag{2}$$

$$\begin{aligned}
e_0 &= \mu c_{r0}(\ell_f + \ell_r)(1 + K)v \\
e_1 &= \mu c_{r0} K(\ell_f + \ell_r)^2 + \ell_f m v^2 \\
e_2 &= K\ell_f(\ell_f + \ell_r)\, mv \\
f_0 &= \mu^2 c_{f0} c_{r0}(\ell_f + \ell_r)^2 + \mu(c_{r0}\ell_r - c_{f0}\ell_f)\, mv^2 \\
f_1 &= \mu(c_{f0}\ell_f + c_{r0}\ell_r)(\ell_f + \ell_r)\, mv \\
f_2 &= \ell_f \ell_r m^2 v^2.
\end{aligned}$$

3. CLOSED LOOP STRUCTURE

Figure 1 shows the structure of the closed loop system upon which the analysis in the following sections is based. It includes some previously published characteristics [1, 2]: Basically it consists of unity feedback of the yaw rate r via an integrator into front wheel steering ($K = 0$, $G_f = 0$, $G_a = 1$, $r_s \to \infty$, $R \to \infty$). This yields robust unilateral decoupling such that the yaw rate r is no longer observable from lateral dynamics at the front axle, in particular from a_f [1]. A faster closed loop dynamics can optionally be achieved by additional feedback of the lateral acceleration at the

front axle a_f with $K > 0$ [1].

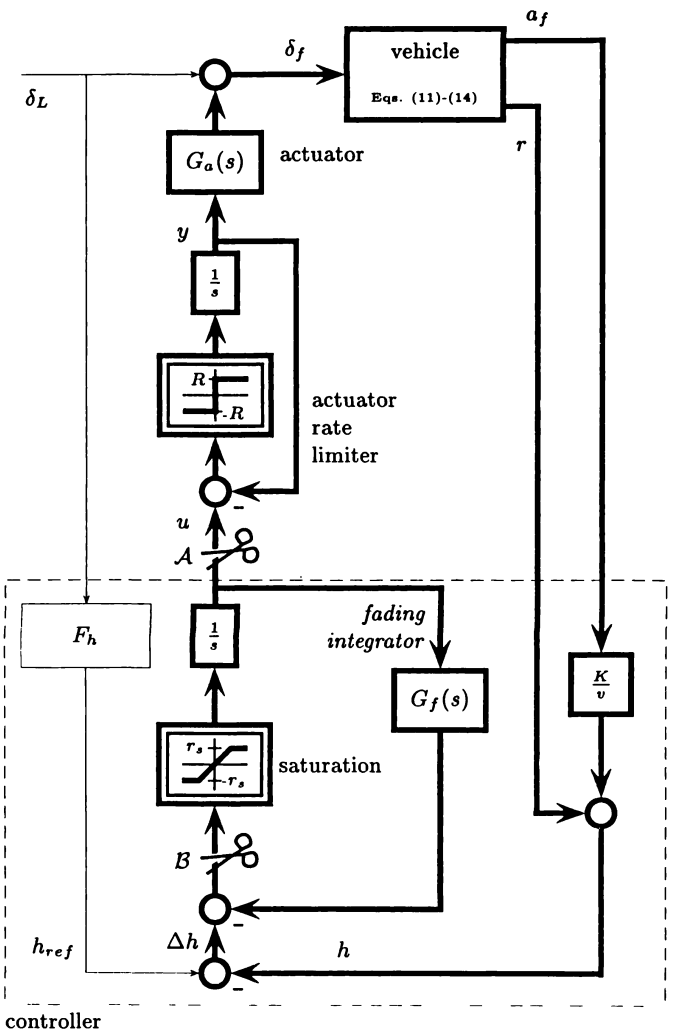

Fig. 1. Closed loop system structure.

By (as well optional) controller-internal feedback of the integrator's output to its input by

$$G_f(s) = \frac{2D_i\omega_i s + \omega_i^2}{s} \tag{3}$$

with $\omega_i = 1/\text{sec}$, $D_i = 1.5$, the integral action is faded out after $\approx 0.5\,\text{sec}$. This modification has been introduced in [2] as *fading integrator* in order to provide disturbance rejection only for about half a second. It helps the driver within his

reaction time but returns to the steady-state behavior of the conventional car afterwards. Neglecting the saturation ($r_s \to \infty$), the transfer function of the fading integrator between Δh and u in Figure 1 is

$$G_i(s) = \frac{1/s}{1 + G_f(s)/s} = \frac{s}{s^2 + 2D_i\omega_i s + \omega_i^2}. \tag{4}$$

For short time ($s \to \infty$), the dynamics is equal to an integrator, however the steady state output ($s \to 0$) is zero and the controlled car has the same steady-state response as the conventional car.

The internal feedback structure allows the limitation of the integrator's input by the saturation element. This further modification will be used in Section 5.

Feedback to the front wheel steering angle is accomplished by an *additional steering angle* actuator with a linear dynamic part which is modelled as

$$G_a(s) = \frac{\omega_a^2}{s^2 + 2D_a\omega_a s + \omega_a^2}. \tag{5}$$

The input to the actuator is filtered by a rate limiter (see Section 4.2) with maximum slope R in order to prevent damage due to overload.

The feedforward path in Figure 1 is marked with thin lines. There is a direct throughput from the steering wheel angle δ_L to the front steering angle δ_f which results in the same initial response to steering wheel inputs as for the conventional ($\delta_f = \delta_L$) car. The set point generation by the dynamic nonlinear filter F_h is of no interest for the investigation in this paper.

4. SINUSOIDAL-INPUT DESCRIBING FUNCTIONS (DFs)

4.1. DF theory

The DF theory [5] is a means to investigate the existence and properties of limit cycles in closed loop systems including linear dynamics $G(s)$ and a static nonlinearity n, which are here assumed in a single loop series connection with negative feedback. One further assumption are distinct low pass properties of the linear dynamics $G(s)$. The DF $N(j\omega, u_0)$ of the nonlinear element n may be considered as the quasi-linear frequency response w.r.t. to the first harmonic of the output for sinusoidal inputs with amplitude u_0.

According to this approximation method a limit cycle with frequency ω is possible for the loop-closing condition (*harmonic balance*)

$$N(j\omega, u_0)\, G(j\omega) = -1 \quad \text{or} \quad G(j\omega) = \frac{-1}{N(j\omega, u_0)}. \tag{6}$$

The latter equation reveals a graphical method to check for limit cycles: Limit cycles are possible, if there are intersection points of the linear part Nyquist plot $G(j\omega)$ and the nonlinear element negative inverse describing function (NIDF) $-1/N(j\omega, u_0)$ in a complex z-plane.

Note that in this paper we are neither concerned with the stability of limit cycles in the sense of their sustentation nor with the state conditions for their appearance nor with their properties (amplitude, frequency). We are only considering the robust avoidance of their possibility in principle.

For the investigations in Sections 5 and 6 the system of Figure 1, including a saturation and a rate limiter, will be used. Therefore, the DFs of these two nonlinear elements are introduced.

4.2. DF of a rate limiter

A rate limiter can be represented by the feedback connection of an integrator and a two-point switching element according to Figure 1 between u and y. The absolute value of the slope of the output y is limited to R.

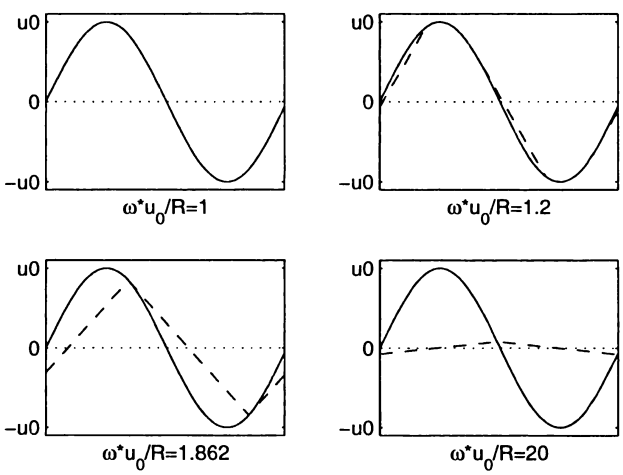

Fig. 2. Rate limiter outputs at various ratios $\omega u_0/R$ for sinusoidal inputs.

Figure 2 shows some steady-state time domain reponses of a rate limiter to sinusoidal inputs. The shape of the output depends on the ratio $\omega u_0/R$ where ω and u_0 are the frequency and amplitude of the input signal respectively. Note that when the rate limiter is activated, the output is reduced in amplitude (down to zero) and delayed in phase (up to $-\pi/2$). The DF of a rate limiter N_a was derived in [4]. Only the result is given here in form of the graphical representation of the NIDF. It is plotted in the complex plane in Figure 3 using gridding along $\omega u_0/R$ and dash-dotted line style.

It starts at $z = -1$ for $\omega u_0/R \leq 1$ and changes over into a straight line ($\mathrm{Re}(z) = -\pi^2/8, \mathrm{Im}(z) < -\pi/4$) for $\omega u_0/R > \sqrt{(\pi/2)^2 + 1}$=1.862.

4.3. DF of a saturation

The DF of a saturation N_s [5] does not depend on the frequency ω, but only on the input amplitude u_{s0}. If the saturation value is reached, there is no phase delay in

the output, only a reduction of the amplitude. The NIDF $-1/N_s$ is -1 if the input amplitude u_{s0} is less or equal to the saturation value r_s and tends to $-\infty$ along the real axis for increasing input amplitudes ($u_{s0}/r_s > 1$), see Figure 3 (dashed line).

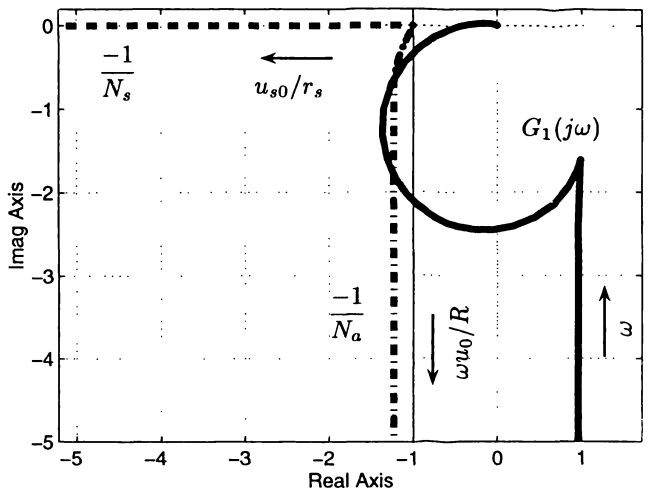

Fig. 3. NIDFs and Nyquist plot for $v = 70\,\mathrm{m/sec}$, $\mu = 1$ (dry road), $K = 0$, $\omega_i = 0$ and $\omega_a = 2\pi \cdot 10\,\mathrm{Hz}$.

5. LIMIT CYCLES DUE TO ACTUATOR RATE LIMITER FOR ROBUSTLY DECOUPLED CAR STEERING DYNAMICS

This section shows, why and under which conditions limit cycles in the closed loop system of Section 3 can occur and introduces a means to significantly reduce the system's susceptibility to limit cycles.

Consider the system of Figure 1 without saturation ($r_s \to \infty$) and cut the loop at $\mathcal{A}$. Then, regarding (2), (4) and (5), the linear part of the open loop transfer function is

$$G_1(s) = G_a(s)\, G_v(s)\, G_i(s). \tag{7}$$

According to Section 4.1, limit cycles can occur, if there are intersection points of the linear part Nyquist plot $G_1(j\omega)$ and the NIDF of the rate limiter $-1/N_a$. The low pass property assumption holds for the considered system G_1 with relative degree three (one from G_i and two from G_a) or four (if K=0, then the relative degree of G_v is one, else zero, see (2)). Generally, the following data are used in this paper:

m=1830kg

c_{f0}=50000N/rad $\quad \ell_f$=1.51m $\quad D_i$=1.5

c_{r0}=100000N/rad $\quad \ell_r$=1.32m $\quad D_a=\sqrt{1/2}$

The controller parameters K, ω_i and the actuator bandwidth ω_a are not yet determined to allow the analysis of their influence. The uncertain plant parameters v, μ may vary within the bounds of an operating domain (see Section 6).

Figure 3 shows a reasonable configuration of controller, actuator, and operating point for which there are intersection points of the Nyquist curve $G_1(s)$ with the NIDF of the actuator rate limiter $-1/N_a$, i.e. limit cycles may occur.

Figure 3 also shows, that the NIDF of a saturation $-1/N_s$ is much less critical for the present case than the rate limiter, because it does not introduce phase delay into the loop.

This leads to the idea suggested in this paper for prevention of limit cycles: It is the introduction of a saturation in front of the integrator as indicated in Figure 1. It can be reliably avoided that the actuator rate limiter reaches its threshold if the derivative of the input to the rate limiter is bounded to a corresponding value. This is achieved by the saturation in front of the integrator (Figure 1) with $r_s \leq R$.

Hence, the actuator rate limiter can be neglected, but the saturation introduced in the controller must be considered. Therefore, cut the loop in Figure 1 at $\mathcal{B}$. The respective open loop transfer function of the linear part is

$$G_2(s) = \frac{1}{s}\left[G_a(s)\, G_v(s) + G_f(s)\right]. \tag{8}$$

For $\omega_i = 0$, $G_2(s) = G_1(s)$ holds. Thus the Nyquist curve in Figure 3 can be directly compared for both cases. As already mentioned, the saturation is less dangerous w.r.t. limit cycles since its NIDF is farer away from the Nyquist curve of the linear system.

It is remarkable, that the existence of limit cycles does not depend on the location of the respective nonlinear element in the (single) loop structure. Thus, for the perfectly integrating control law ($\omega_i = 0$), it does not make any difference, whether the saturation occurs in front of the integrator or behind the actuator. For that reason, also a saturation behind the actuator (not modeled in Figure 1) is covered by the analysis. The analysis becomes more sophisticated, however, for the fading integrator. In this case there are two nonlinear elements to be considered in two loops (not covered by this paper).

6. VERIFICATION OF ROBUST LIMIT CYCLE AVOIDANCE IN PARAMETER SPACE

Now, since the NIDF of the rate limiter $-1/N_a$ in Figure 3 is no more relevant, the respective system belonging to the plotted Nyquist curve is not able to perform limit cycles. There are no intersection points with the NIDF of the saturation $-1/N_s$. But how about changed parameters $v, \mu, K, \omega_i, \omega_a$? Of course, the avoidance of limit cycles must be robust w.r.t. the uncertain or varying parameters of the plant.

The approach which is used in this paper to verify robust prevention of limit cycles combines the theory of DFs with the parameter space approach. The idea is the following:

The parameters K, ω_i and ω_a are considered as fixed parameters. We assume there is an operating point $P = (v_p, \mu_p)$ where there is no intersection between

$G_2(j\omega)$ and $-1/N_a$, i.e. P is *limit-cycle-free*. Then we determine the neighborhood of P in the (v, μ)-parameter plane which is also limit-cycle-free. If this region includes the operating domain of the plant, then we call the controlled system *robustly limit-cycle-free*.

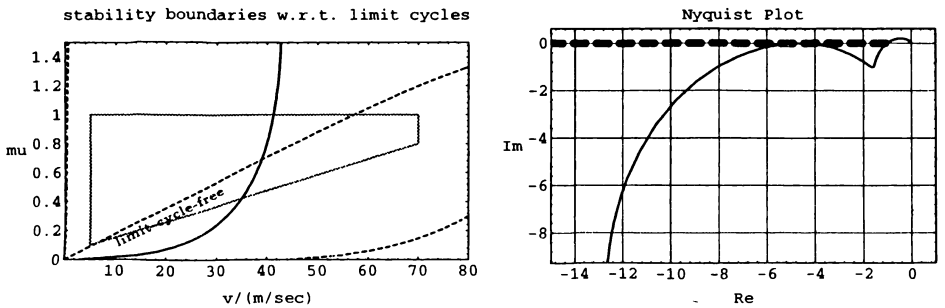

Fig. 4. $\omega_a = 2\pi \cdot 2\,\text{Hz}$, $K = 19$, $\omega_i = 0$,
(Nyquist plot: $v = 38.75\,\text{m/sec}$, $\mu = 0.685$ (wet road)).

The limit-cycle-free region is separated from the neighboring *limit-cycle-tainted* regions by borders. These borders are generated by mapping respective conditions formulated in terms of the Nyquist plot into the (v, μ)-parameter plane.

The Nyquist plot in Figure 4 illustrates two different conditions at the same time, under which the closed loop system may evolve from "limit-cycle-free" to "limit-cycle-tainted". The NIDF of the saturation $-1/N_s$ (plotted with dashed line style) starts at the critical point -1. Thus the Hurwitz stability border ($G_2(j\omega) = -1$) at the same time is a border for the system to turn from "limit-cycle-free" into 'limit-cycle-tainted", hence denoted as *Hurwitz condition*. Mathematically this may be expressed by

$$\text{Re } G_2(j\omega) = -1 \quad \text{and} \quad \text{Im } G_2(j\omega) = 0. \tag{9}$$

Theoretically, there is also a real root condition for $G_2(0)$. In the case of the present system, however, this condition is not active because $\text{Im } G_2(0) = -\infty$.

For the second possible condition, the *tangent condition*, the Nyquist curve touches $-1/N_s$ horizontally, i.e.

$$\begin{gathered} \text{Im } G_2(j\omega) = 0 \quad \text{and} \quad \frac{\partial \,\text{Im } G_2(j\omega)}{\partial \omega} = 0 \\ \text{observing} \quad \text{Re } G_2(j\omega) \leq -1. \end{gathered} \tag{10}$$

The resultant of (9) can be used, to map the Hurwitz-stability boundaries into the (v, μ)-parameter plane [1]. The symbolic and numeric computations may be accomplished by the Matlab-based toolbox PARADISE [8]. In the parameter plane, a finite number of regions is generated which are separated by the mapped boundaries. One or more of these regions may turn out to be Hurwitz-stable.

The same kind of mapping may be applied to the tangent condition. The boundaries in parameter space are generated by solving the resultant of the two equations

in (10). The inequality must be taken into account when determining limit-cycle-free solutions. Again, a finite number of regions are generated in the parameter plane (see Figure 4, left plot). The scope of the analysis in parameter space is, to find out, whether the system is limit-cycle-free in the entire operating domain or not. If there are no boundaries (coming from any of the two conditions) intersecting the operating domain and an arbitrary operating point in the operating domain turns out to be limit-cycle-free, then the system is robustly limit-cycle-free. Otherwise, the test for robust limit cycle avoidance fails.

Consider Figure 4 as example. The left plot shows the boundaries between limit-cycle-free and limit-cycle-tainted regions in the (v, μ)-parameter plane for a low bandwidth actuator ($\omega_i = 2\pi \cdot 2\,\mathrm{Hz}$) and high controller gain ($K = 19$) with genuine integral action ($\omega_i = 0$). The Hurwitz condition boundaries are plotted with dashed line style, solid line style is used for tangent condition boundaries. The operating domain of the car is plotted as a polygon. The right plot shows the Nyquist curve for the operating condition which corresponds to the intersection point of the two different type boundaries in the middle of the operating domain. Here both conditions for passing over a border can be simultaneously seen. Only the lower left part of the operating domain turns out to be limit-cycle-free, all other regions are limit-cycle-tainted. Since the operating domain is not completely included in the limit-cycle-free region, this system is not robustly limit-cycle-free.

Figures 5 and 6 show two more interesting cases which anticipate the actuator bandwidth specification in the next section.

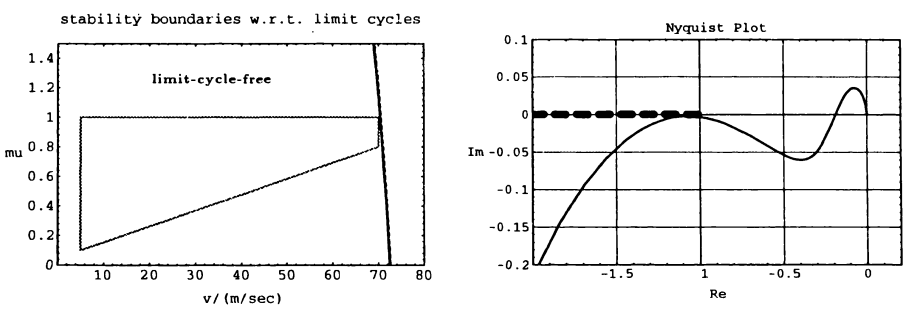

Fig. 5. $\omega_a = 2\pi \cdot 3.3\,\mathrm{Hz}$, $K = 4$, $\omega_i = 0$, (Nyquist plot: $v = 70\,\mathrm{m/sec}$, $\mu = 1$ (dry road)).

In Figure 5 the genuine decoupling controller with a_f-feedback ($\omega_i = 0$, $K = 4$) and an actuator bandwidth $\omega_a = 2\pi \cdot 3.3\,\mathrm{Hz}$ is investigated. Two boundaries are very close to the operating domain at high speed on dry road. This example exhibits an almost-simultaneous fulfillment of both the Hurwitz and the tangent condition at one operating point (v=70 m/sec, μ=1). As can be seen from the right plot in Figure 5, the Nyquist curve almost touches the real axis very close to -1. The boundaries which correspond to the two different conditions are very close to each other, so that they can hardly be distinguished in the parameter plane.

For the example in Figure 6 the gain for a_f-feedback is increased ($\omega_i = 0$, $K = 9$)

and a high bandwidth actuator is used ($\omega_a = 2\pi \cdot 10\,\mathrm{Hz}$).

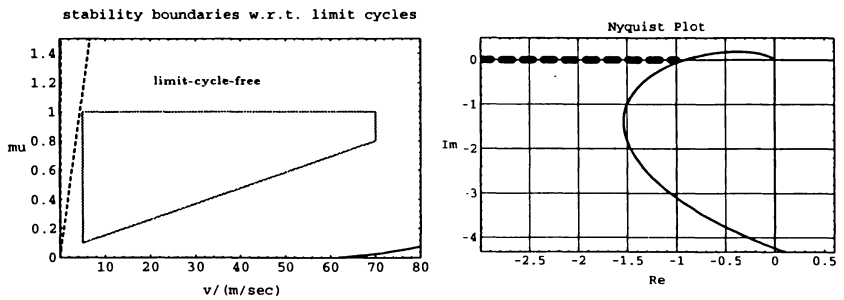

Fig. 6. $\omega_a = 2\pi \cdot 10\,\mathrm{Hz}$, $K = 9$, $\omega_i = 0$, (Nyquist plot: $v = 5\,\mathrm{m/sec}$, $\mu = 1$ (dry road)).

Now, low speed on dry road appears to be the most critical operating condition. If a slower actuator is used, the system violates Hurwitz stability and is limit-cycle-tainted at least at this operating point.

6.1. Application example: Actuator bandwidth specification

Now, the described approach is used to validate robust prevention of limit cycles for various controller versions. For each controller, a respective actuator bandwidth had been found in a preliminary iteration, such that the system is robustly limit-cycle-free, but at least one boundary is very close to the operating domain (as in the examples of Figures 5 and 6). Thus a minimum required actuator bandwidth is specified. The specification and the validation of robustness is repeated for each controller.

Table 1. Minimum required actuator bandwidth $\omega_{a,\min}$ $[2\pi \cdot \mathrm{Hz}]$

	$K = 0$	$K = 4$	$K = 9$
$\omega_i = 0$	3.15	3.3 (Figure 5)	10 (Figure 6)
$\omega_i = 1/\mathrm{sec}$	1.3	1.66	8.5

The first controllers do not make use of fading out the integral action ($\omega_i = 0$), but the feedback gain for lateral acceleration a_f at the front axle is varied in three steps. The same variation is repeated for a controller with the fading integrator ($\omega_i = 1/\mathrm{sec}$). Table 1 shows the results.

Generally, it can be stated, that the employment of the fading integrator reduces the susceptibility to limit cycles, if compared to the perfect integrator. Or, in other words, only a slower actuator is necessary to robustly avoid limit cycles. This is quite evident, since the fading activity reduces the low frequency demand on the actuator.

Increasing the closed loop gain by augmentation of K, on the other hand, requires a higher minimum actuator bandwidth, if limit cycles shall be robustly avoided.

7. CONCLUSIONS

In this paper a combination of the parameter space method and the theory of describing functions has been used to investigate the robust prevention of limit cycles of a single loop system containing a nonlinear element. The described method has been succesfully applied to the example of an actively steered car. The susceptibility of the controlled car to limit cycles has been reduced by adapted replacement of nonlinearity characteristics. For the resulting plant and different controller versions, the approach has been used to specify the minimum required bandwidth of the steering actuator. It turns out, that the assignment of fading activity to the decoupling integrator in the controller reduces the actuator bandwidth requirements. On the other hand, increasing the closed loop gain makes the expenditure of a faster actuator necessary to robustly avoid the risk of limit cycles. Note, however, that the actuator specification here only examines the question of limit cycle avoidance. No other closed loop requirements (e. g. damping of system eigenvalues etc.) are considered.

Appendix A: Linear car model

The car model which is used for the investigations in this paper is the classical linearized single track model [6] as illustrated in Figure 7.

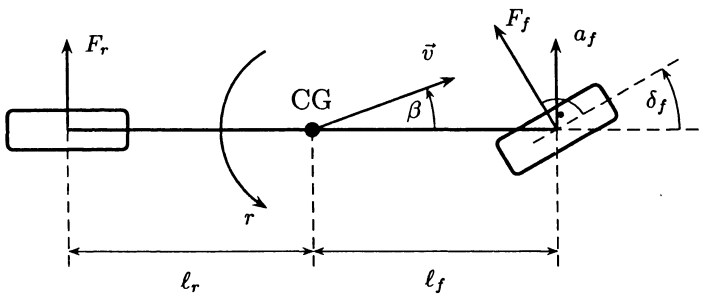

Fig. 7. Single-track model.

Its major quantities are

$F_f(F_r)$	lateral wheel force at front (rear) wheel
r	yaw rate (measured by a gyro)
β	chassis side slip angle at center of gravity (CG)
$\vec{v}$	velocity vector at CG
v	magnitude of $\vec{v}$ $(v > 0,\ \dot{v} = 0)$
a_f	lateral acceleration at the front axle
$\ell_f(\ell_r)$	distance from front (rear) axle to CG
δ_f	front wheel steering angle

The mass of the vehicle is m and J is the moment of inertia w.r.t. a vertical axis through the CG. Here socalled *ideal mass distribution* [1, 3] is assumed, i. e.

$J = m\ell_f\ell_r$, which as an approximation holds for most passenger cars. For small steering angle δ_f and small side slip angle β, the equations of motion are [1, 7]

$$\begin{bmatrix} mv(\dot{\beta} + r) \\ m\ell_f\ell_r\dot{r} \end{bmatrix} = \begin{bmatrix} F_f + F_r \\ F_f\ell_f - F_r\ell_r \end{bmatrix}. \tag{11}$$

The tire force characteristics are linearized as

$$F_f(\alpha_f) = \mu c_{f0}\alpha_f, \quad F_r(\alpha_r) = \mu c_{r0}\alpha_r \tag{12}$$

with the tire cornering stiffnesses c_{f0}, c_{r0}, the road adhesion factor μ, and the tire side slip angles

$$\alpha_f = \delta_f - (\beta + \frac{\ell_f}{v}r), \quad \alpha_r = -(\beta - \frac{\ell_r}{v}r). \tag{13}$$

The lateral acceleration at the front axle is

$$a_f = v(\dot{\beta} + r) + \ell_f\dot{r}. \tag{14}$$

(Received April 8, 1998.)

REFERENCES

[1] J. Ackermann, A. Bartlett, D. Kaesbauer, W. Sienel and R. Steinhauser: Robust control: Systems with uncertain physical parameters. Springer, London 1993.

[2] J. Ackermann and T. Bünte: Automatic car steering control bridges over the driver reaction time. Kybernetika *33* (1997), 61–74, also in Proc. 3rd IEEE Mediterranean Symposium on New Directions in Control and Automation, Limassol 1995, pp. 293–300.

[3] J. Ackermann, T. Bünte, W. Sienel, H. Jeebe and K. Naab: Driving safety by robust steering control. In: Proc. Internat. Symposium on Advanced Vehicle Control, Aachen 1996.

[4] H. Duda: Effects of rate limiting elements in flight control systems – a new PIO criterion. In: Proc. AIAA Guidance, Navigation, and Control Conference, Baltimore 1995.

[5] A. Gelb and W. van der Velde: Multiple-Input Describing Functions and Nonlinear System Design. MacGraw-Hill, New York 1968.

[6] P. Riekert and T. Schunck: Zur Fahrmechanik des gummibereiften Kraftfahrzeugs. Ingenieur Archiv *11* (1940), 210–224.

[7] M. Mitschke: Dynamik der Kraftfahrzeuge, Vol. C. Springer, Berlin 1990.

[8] W. Sienel, J. Ackermann and T. Bünte: Design and analysis of robust control systems in PARADISE. In: Proc. IFAC Symposium on Robust Control Design, Budapest 1997.

Prof. Dr.-Ing. Jürgen Ackermann and Dipl.-Ing. Tilman Bünte, DLR, German Aerospace Center, Institute of Robotics and System Dynamics, Oberpfaffenhofen, D-82230 Wessling. Germany.

e-mail: juergen.ackermann@dlr.de